NASA/TM—2013–216625

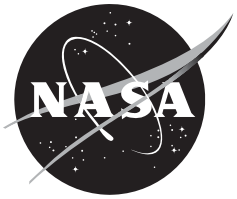

IDENTIFICATION OF NOISE SOURCES DURING ROCKET ENGINE TEST FIRINGS AND A ROCKET LAUNCH USING A MICROPHONE PHASED-ARRAY

Jayanta Panda

Ames Research Center, Moffett Field, California

Robert N. Mosher
NASA Langley Research Center, Hampton, VA

Barry J. Porter
Aerospace Computing Inc., Mountain View, CA

December 2013

NASA STI Program ... in Profile

Since its founding, NASA has been dedicated to the advancement of aeronautics and space science. The NASA scientific and technical information (STI) program plays a key part in helping NASA maintain this important role.

The NASA STI program operates under the auspices of the Agency Chief Information Officer. It collects, organizes, provides for archiving, and disseminates NASA's STI. The NASA STI program provides access to the NASA Aeronautics and Space Database and its public interface, the NASA Technical Reports Server, thus providing one of the largest collections of aeronautical and space science STI in the world. Results are published in both non-NASA channels and by NASA in the NASA STI Report Series, which includes the following report types:

- TECHNICAL PUBLICATION. Reports of completed research or a major significant phase of research that present the results of NASA Programs and include extensive data or theoretical analysis. Includes compilations of significant scientific and technical data and information deemed to be of continuing reference value. NASA counterpart of peer-reviewed formal professional papers but has less stringent limitations on manuscript length and extent of graphic presentations.

- TECHNICAL MEMORANDUM. Scientific and technical findings that are preliminary or of specialized interest, e.g., quick release reports, working papers, and bibliographies that contain minimal annotation. Does not contain extensive analysis.

- CONTRACTOR REPORT. Scientific and technical findings by NASA-sponsored contractors and grantees.

- CONFERENCE PUBLICATION. Collected papers from scientific and technical conferences, symposia, seminars, or other meetings sponsored or co-sponsored by NASA.

- SPECIAL PUBLICATION. Scientific, technical, or historical information from NASA programs, projects, and missions, often concerned with subjects having substantial public interest.

- TECHNICAL TRANSLATION. English-language translations of foreign scientific and technical material pertinent to NASA's mission.

Specialized services also include organizing and publishing research results, distributing specialized research announcements and feeds, providing information desk and personal search support, and enabling data exchange services.

For more information about the NASA STI program, see the following:

- Access the NASA STI program home page at http://www.sti.nasa.gov

- E-mail your question to help@sti.nasa.gov

- Fax your question to the NASA STI Information Desk at 443-757-5803

- Phone the NASA STI Information Desk at 443-757-5802

- Write to:
  STI Information Desk
  NASA Center for AeroSpace Information
  7115 Standard Drive
  Hanover, MD 21076-1320

NASA/TM—2013–216625

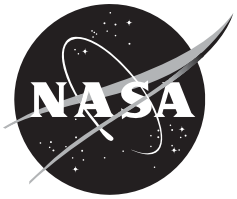

IDENTIFICATION OF NOISE SOURCES DURING ROCKET ENGINE TEST FIRINGS AND A ROCKET LAUNCH USING A MICROPHONE PHASED-ARRAY

Jayanta Panda

Ames Research Center, Moffett Field, California

Robert N. Mosher
NASA Langley Research Center, Hampton, VA

Barry J. Porter
Aerospace Computing Inc., Mountain View, CA

National Aeronautics and
Space Administration

Ames Research Center
Moffett Field, CA 94035-1000

December 2013

Acknowledgments

The authors would like to thank Mr. Roberto Garcia of NASA Marshall Space Flight Center and Mr. Nans Kunz of Ames Research Center for partially funding this work. Additional support was provided by NASA ASP innovative measurements program. Mr. Jeff Reddish and Mr. Mark Cording of the Wallops Flight Facility, Mr. Kevin Meehan of NASA Johnson Space Center, and Mr. Kurt Eberly and Mr. Tony Gaio of the Orbital Sciences Corporation were instrumental in coordinating this multi-agency effort. We benefited greatly from the engineering advice that Mr. Mark Cording provided. We would also like to thank Mr. Ted Garbeff for performing the modeling work for optimizing the microphone locations, Ms. Laura Kushner for photogrammetric verification of these locations, and Mr. Greg Zilliac for allowing us to setup the array during the hybrid rocket tests. Finally, the credit for the high-speed camera photos of Fig 11 goes to the NASA imagery group at Kennedy Space Center (KSC-KX).

IDENTIFICATION OF NOISE SOURCES DURING ROCKET ENGINE TEST FIRINGS AND A ROCKET LAUNCH USING A MICROPHONE PHASED-ARRAY

J. Panda
NASA Ames Research Center, Moffett Field, CA

R. N. Mosher
NASA Langley Research Center, Hampton, VA

B. J. Porter
Aerospace Computing, Inc, Mountain View, CA

A 70 microphone, 10-foot by 10-foot, microphone phased array was built for use in the harsh environment of rocket launches. The array was setup at NASA Wallops launch pad 0A during a static test firing of Orbital Sciences' Antares engines, and again during the first launch of the Antares vehicle. It was placed 400 feet away from the pad, and was hoisted on a scissor lift 40 feet above ground. The data sets provided unprecedented insight into rocket noise sources. The duct exit was found to be the primary source during the static test firing; the large amount of water injected beneath the nozzle exit and inside the plume duct quenched all other sources. The maps of the noise sources during launch were found to be time-dependent. As the engines came to full power and became louder, the primary source switched from the duct inlet to the duct exit. Further elevation of the vehicle caused spilling of the hot plume, resulting in a distributed noise map covering most of the pad. As the entire plume emerged from the duct, and the on-deck water system came to full power, the plume itself became the loudest noise source. These maps of the noise sources provide vital insight for optimization of sound suppression systems for future Antares launches.

Nomenclature:

b = Beamformed output (dB)
w = Steering vector
$i = \sqrt{-1}$
M = Total no of microphones
Γ = Coherence
G = Cross-spectral matrix
R = Radial position of microphone from array center (in)
S = Weight applied to individual microphones
θ = Angular position from the image center (rad)
λ = Wavelength (ft)
d = Aperture of the array (ft)
f = Frequency (Hz)
< > = Expected value
c = speed of sound (ft/s)
k = wavenumber = $2\pi f / c$ (1/ft)
N, N_s = No of grid points in the viewing region
r = *distance of a microphone from a source (interrogation point)*
t = time from engine ignition (s)
α = strength of monopole sources

Superscripts:

† = Complex-conjugate and transpose
*** =** Complex conjugate only
T = Transpose only
mod = model

Subscripts:

c = center of the array
j = index for interrogation grid
m = microphone index
R = Rayleigh resolution

Acronym:

TEL = Transporter Erector Launcher
psf = point-spread-function

I. INTRODUCTION

Every part of a launch vehicle, launch pad and ground operation equipment are subjected to the high acoustic load generated during lift-off. The acoustic load is a major contributor to the vibro-acoustics environment to which every payload, vehicle structure, propellant storage and handling devise, electronics and navigational components have to be designed, tested and

certified. Even a couple of decibel reduction of the acoustic level translates into a sizable reduction of cost of certification, operation and the weight of vehicle. The same is true for every payload that vehicle carries. Therefore, the lowering of the acoustic level via various mitigation schemes is an important aspect of a launch pad design. The first step towards the evaluation of any mitigation process is an identification of the sources responsible for noise generation. The present work is part of an instrumentation development program to identify launch acoustic sources. Typically, single microphones are placed at different locations on a launch pad to measure acoustic fluctuations. Such microphones, however, are unable to determine the sources. Single microphones provide a measure of the absolute level on the vehicle and other places, leaving the cause of noise generation to speculations. In contrast, a phased array of microphones along with beam-form processing directly identifies the location and strength of the noise sources, and is therefore capable of providing significant insights into the underlying cause.

The present effort is a continuation of the prior work [1, 2] where a smaller size microphone phased array was used in model-scale launch acoustic tests. A 5% scaled model of the ARES I vehicle was tested in a static firing to determine the noise sources with different types of water injection and different elevations of the vehicle. The results provided significant insight into the source distribution which was found to be very different from that used for traditional models [3, 4]. The goal of the present work was to take the phased array development to the next level, i.e., application to a full-scale rocket vehicle. The array was used for both a static test fire and actual launch. The work presented in this report was a multi-year effort that started with the design of a large aperture phased array suitable for the lower frequencies of interest in a full-scale vehicle. The larger aperture is also suitable for placing the array at a greater distance from the launch pad. The design of the new large-aperture phased array had conflicting requirements for a lightweight structure for ease of transportation, and a sturdy structure to house sensitive equipment in the harsh environment of a launch site. The newly built array was then tested in an anechoic chamber, and then in a small rocket engine test facility. New data processing software were developed to perform beamforming for the transient noise sources seen during the rocket launch. Finally all parts were sent to the NASA Wallops Flight Facility for setup near the Antares launch pad where the array was rebuilt and deployed during the Antares engine test fire and launch. The present paper is a summary report from all these activities; although more emphasis is placed on results from Antares launch.

The only prior application of a set of microphones used for beamforming during an actual rocket launch was by Gély et al [5]. However, the premise was vastly different. They attached 12 microphones distributed around the large payload fairing of the Ariane V vehicle during one of its first launches, and applied beamform processing to the flight data. The noise maps, albeit of poor resolution, confirmed the source distribution found during a model-scale static-fire test. In principle, any set of microphones can be used as a phased array as long as the time signals are synchronized, and the microphone locations are known within a fraction of the sound wavelength. The present work differs significantly from the prior efforts. Much higher resolution maps of the noise sources were obtained by an optimized planar array which was placed on the launch pad rather than on the flight vehicle. This also reduced the cost of operation; ground sensors cost a small fraction of that of the flight sensors. A phased array resolves sources of sound waves that impinge on the array. Ideally a payload fairing mounted array is suitable to find sources that specifically radiate towards the payload which perhaps was the motivation of Gély et al [5]. However, the cylindrical shape of the fairing does not allow for optimal placement of the microphone sensors, leading to poor resolution. Most noise sources of interest to rocket launches radiate in all directions (albeit non-uniformly).The results obtained from the present effort are expected to be applicable to all parts of launch operation, and particularly suitable to optimize the acoustic attenuation systems. Other goals of the present effort are to verify the noise source models used in the traditional empirical prediction methods [3, 4] and to provide a comparison case for the more recent efforts to predict launch acoustics via computational aero-acoustics [6, 7].

Ia. Antares Vehicle and NASA Wallops pad 0A:

Antares is a two-stage, medium class (5000kg) commercial launch vehicle, built and operated by Orbital Sciences Corporation. The first stage is comprised of twin NK-33 (AJ-26) based liquid oxygen and kerosene (RP1) engines that produced 3265kN of thrust, and the second stage is a single ATK castor solid motor. The hot-fire static engine test and the maiden launch occurred from pad 0A of Mid-Atlantic Regional Spaceport located at NASA Wallops Flight Facility. The launch pad was extensively modified for the engine test and the launch which were first ever from this modified pad. A wheeled Transporter Erector Launcher (TEL) was used to roll out and erect the rocket on its launch pad. The TEL also acted as the rocket's gantry and was tilted back to release the vehicle during launch.

Figure 1 presents a collage of photographs showing the location of the phased array with respect to the launch pad. An examination of the photos shows the details of launch operation relevant to the present discussion. Figure 1(a) was from the instance when Antares was on the verge of lift-off; the engines came to full power and the glow of the plume was visible through the holes of the launch mount. The TEL was tilted back and the vehicle was released. The vehicle was mounted on the top of a flame duct with a single hole and a J-deflector. Plumes from the twin engines flowed over the deflector and exit out through the duct outlet away from the vehicle, towards the ocean. In order for the plume to go over a nearby sea-wall the trench outlet was slanted upward by a nominal 10° angle. Figure 1(a) shows the ejection of a large amount of steam, water and plume gases through the duct exit. Figure 1(b) is from a later instant of time when the vehicle lifted off with a long trail from the plumes. Figure 1(c) was from an earlier static-fire test of the first stage engine. The first stage and a part of the TEL were on the pad. The engines were mounted on the same duct but on a different, taller, engine mount suitable for the long static burn. Additional details of the launch will be proved later in the text.

The pad was equipped with an acoustic suppression system made of three different sets of water injection ports. A large tank (Fig 1a) was built next to the pad to supply this water. Figure 2 (a) shows the first set of ports around the duct inlet. The second one was inside the duct and sprayed water on the J-deflector. The 'duct water' started to flow before engine ignition. The third set of nozzles, called "rainbirds", sprayed water on the top of the launch pad (Fig 2b). The "rainbird" system also helped to protect the deck from plume impingements. The individual rainbird heads are also visible in Fig 2(a). There were two sets of rainbirds, the shorter ones started early while the longer ones were delayed to avoid deluging the bottom of the vehicle.

II. DESIGN AND CONSTRUCTION OF THE MICROPHONE PHASED ARRAY

A rule of thumb to select the array aperture for a desirable source resolution can be found from the Rayleigh criterion. For a circular aperture of diameter d, the minimum resolvable angular separation (in radians) θ_R between two sources is directly related to the wavelength via the following relation:

$$sin\theta_R = 1.22\,\frac{\lambda}{d} \qquad \textbf{(1)}$$

The above equation is mostly satisfied by the conventional beamform procedure, although various authors have claimed superior resolution using different deconvolution procedures. Judicious positioning of the microphones also helps to improve the resolution. Nonetheless, Eq 1 provides guidance in selecting the size of the array. The new 10-foot by 10-foot array has an aperture three times larger than the older one used in the model scale test [1, 2]. Figure 3 shows the layout of the microphones on the array face.

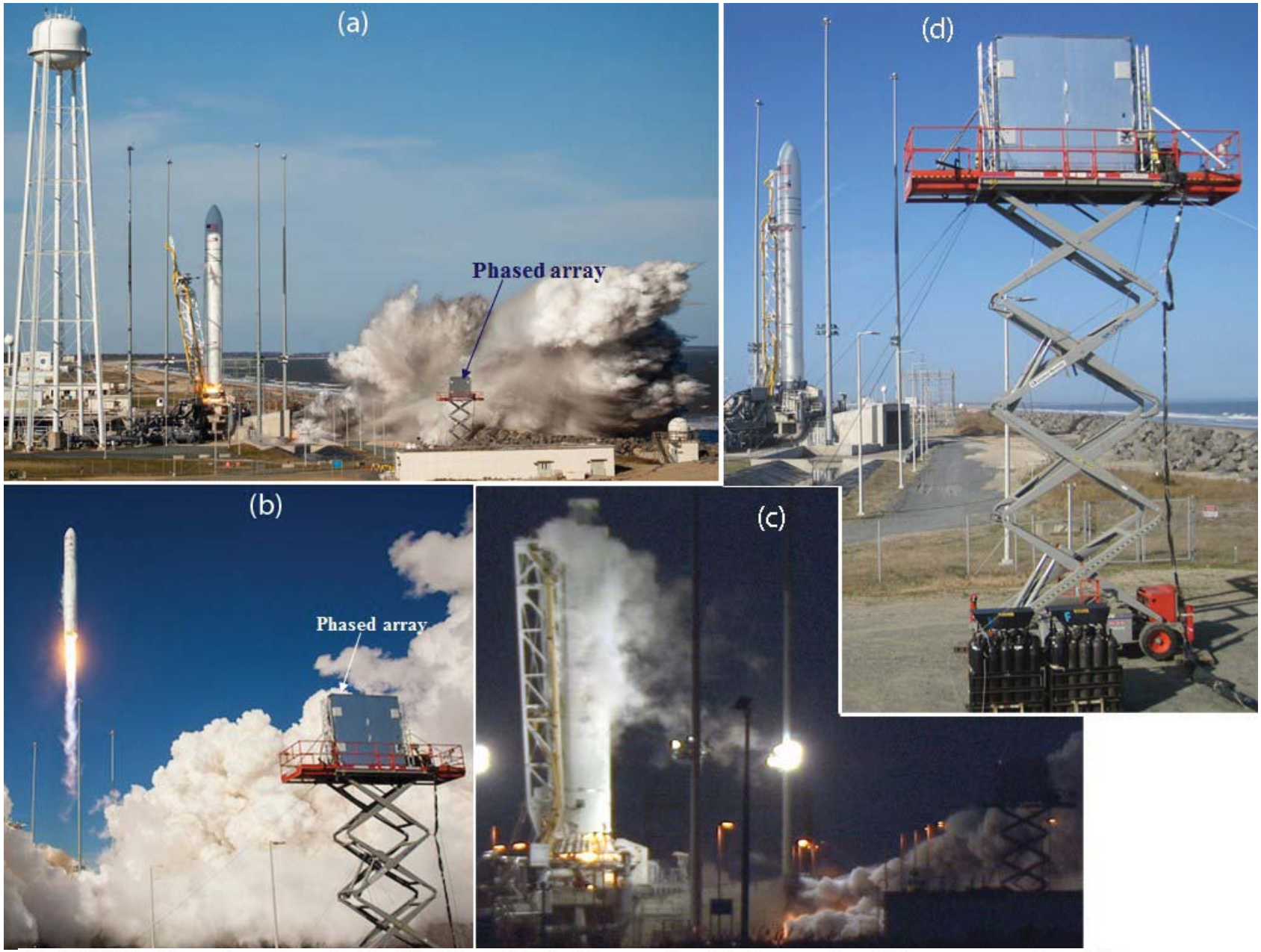

Fig. 1 (a), (b) Antares A-one launch; (c) static firing of the first-stage engine; (d) close-up view of the array on a scissor-lift.

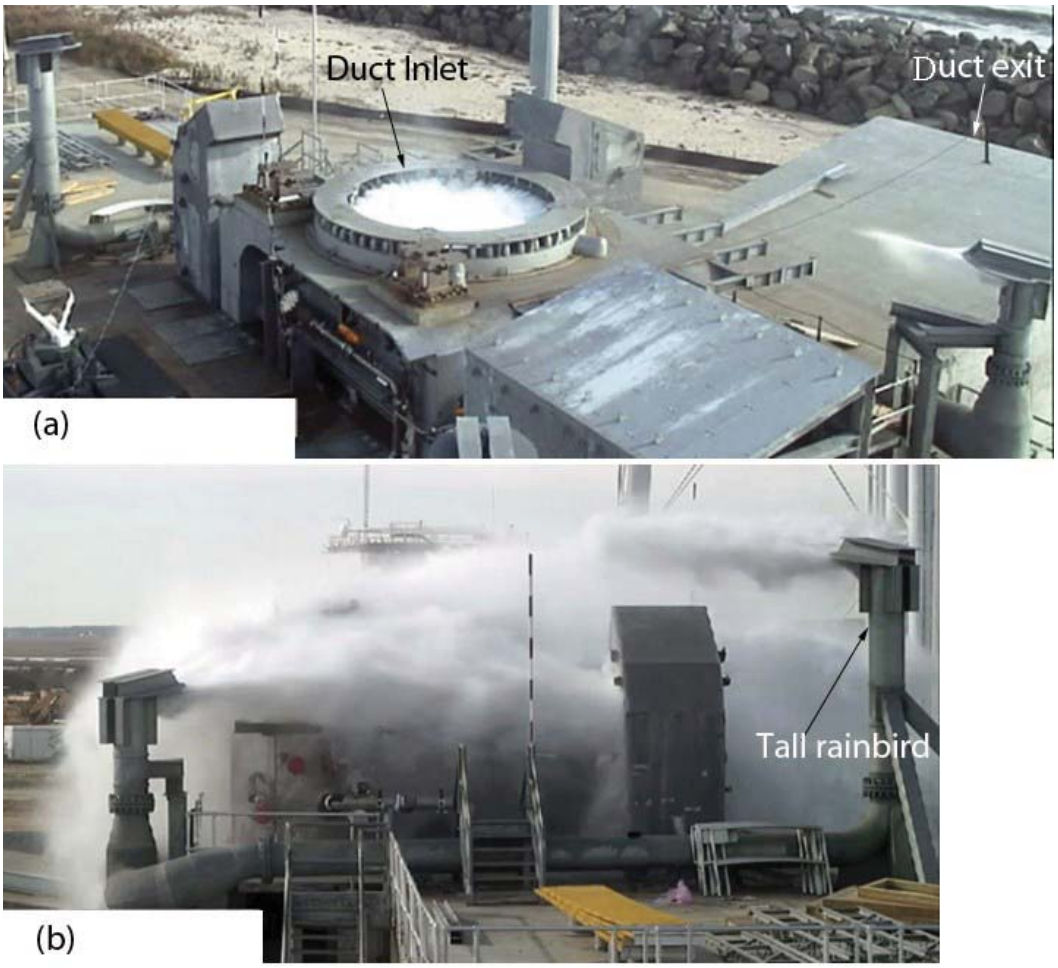

Fig. 2 *Water injection systems used for acoustic attenuation in launch pad 0A. (a) Duct inlet water (view from the south-west side); (b) on-deck "rainbird" water (view from the east side).*

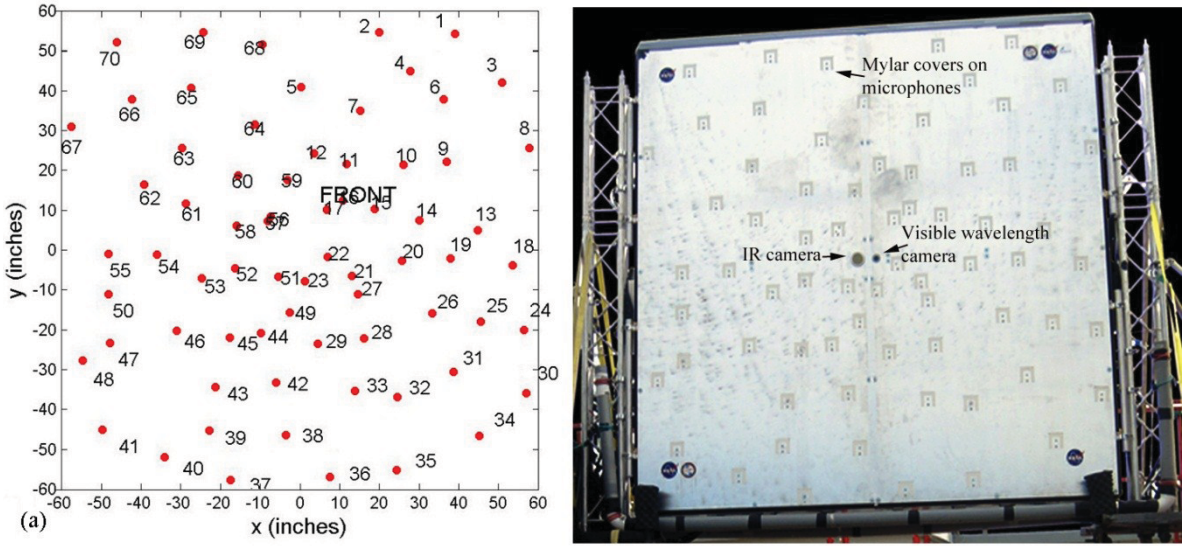

Fig. 3 *(a) Microphone layout and (b) a photograph of the front surface of the 10-foot by 10-foot array.*

The goal of the microphone layout was to maximize the array resolution at the lower 400Hz ≤ f ≤ 2 kHz range, while also reducing the side lobes. The total number of microphones was limited to 70, and the available area limited to a 10ft X 10ft square. Two other constrains were necessary: adjacent pairs of microphones could not be closer than 0.5 inches, and no microphones could occupy the space within a six-inch diameter circle at the center of the plate. The first criterion was for ease in microphone placement, and the second was to reserve the array center for two cameras. To design the layout, the first 56 microphones were placed on five different logarithmic spirals [8]. The starting points of the spirals were placed on an ellipse centered at the middle of the plate. Since the spirals did not fill the corners of the square plate, additional 16 microphones were placed along the outer edges of two ellipses, whose major axes were along the diagonals of the 10'X10' square. The pattern turned out to produce a fairly narrow point-spread function (psf). The optimization of these initial locations was performed via a "simulated annealing process" using Matlab® codes that provided further improvements. The cost function used for the optimization procedure was a sum of the angular extent for 3dB resolution plus side-lobe rejection (i.e., the difference between the primary peak and the next highest peak in psf) at 750Hz. The optimization process distorted the original spirals and ellipses and was found to sharpen the psf. interestingly the center starting ellipse was optimized to a circle. Table I shows the final microphone coordinates. At 750 Hz, the 3dB resolution of the array is 4.12° and the side-lobe reject is 14.8dB. The microphone layout provided a greater resolution at low frequency (400 Hz) in exchange for increased side-lobes at high frequency (5 kHz). Since the goal was for an improved resolution for f ≤2 kHz, the design suits our purpose. It is believed that the same coordinates can be linearly scaled to any other array size, as long as the number of microphones is kept to 70. The optimum design frequency of 750Hz is also expected to scale accordingly. The theoretical psf at two different frequencies are shown in Figs 4(a) and 4(c). Figure 4(b) and 4(d) present the measured response in an anechoic chamber from a single speaker source placed 61.5 feet away from the array. The source maps are superimposed on a photograph taken by the video camera at the center of the array. The drawn-curtain shape of the image is due to the barrel correction applied on the photo. Figure 4 show favorable comparison between the theoretical and measured psf. This provides confidence in the array setup and the software used for data analysis.

The 10-foot by 10-foot array chamber housed all sensors and the cameras (Fig 3b). To provide protection from the environmental elements and the debris field the amplifiers, data acquisition systems and computers were packaged for a separate housing. The two units were connected by a 164 feet long weather-protected cable bundle that was passed through conduits. The data and image acquisition computers were accessed over a local area network from a remote location using separate laptop computers. The 70 G.R.A.S. ® ¼ inch, condenser microphones with protection grids were flush mounted on the front side of the array box. Every microphone was calibrated using a piston phone, and phase-checked with respect to a fixed microphone. The array box also held one visible wavelength camera, one infrared wavelength thermal camera, and one two-axis accelerometer. The 1.3Mpixel visible wavelength camera was useful to determine the look-angle of the array and also for remote observation. The 640X480 pixels, long infra-red, thermal imaging camera provided a view of the flow path for the hot-plume which otherwise was obscured by the steam and debris generated during launch. The two cameras were at the center of the array behind windows. The accelerometer provided a measure of the vibration levels of the array chamber, and was mounted in one of the cable junction boxes. The thermal imaging camera was found to be prone to failure from excessive vibration. A special vibration isolation mount was created for the launch; the camera ultimately failed but provided data for the first 15sec which was of interest for the present investigation.

While maintaining sufficient sturdiness, the requirement was to keep the labor required to assemble, transport, disassemble, pack, and ship the array to a minimum. To satisfy these goals the array chamber was made of lightweight aluminum honeycomb sandwich panels and a lightweight metal frame. No individual frame piece or panel weighed more than 60 lbs., allowing

full assembly without the use of cranes. Weather stripping and silicone sealants were applied to the panels to help waterproof the enclosure. In order to mount the array box enclosure in position for a test, clamps were bolted through the internal aluminum frame, and were attached to aluminum trusses (similar to those used in mounting stage lights). The trusses could be mounted to either flat steel plate bases or to mobile bases having casters and supporting outrigger assemblies for stability.

Table I. ***Coordinates of the microphone sensors on the array***

Mic no	X (in)	Y (in)	Mic no	X (in)	Y (in)	Mic no	X (in)	Y (in)	Mic no	X (in)	Y (in)
1	39.038	54.320	**19**	37.832	-2.063	**37**	-17.522	-57.649	**55**	-48.177	-0.957
2	19.888	54.582	**20**	25.713	-2.580	**38**	-3.475	-46.473	**56**	-7.293	8.372
3	50.969	42.057	**21**	13.167	-6.431	**39**	-22.849	-45.299	**57**	-8.114	7.340
4	27.719	44.828	**22**	7.012	-1.638	**40**	-34.087	-52.037	**58**	-15.909	6.079
5	0.240	40.952	**23**	1.291	-7.824	**41**	-49.729	-45.119	**59**	-3.087	17.649
6	36.110	37.818	**24**	56.511	-20.142	**42**	-6.053	-33.179	**60**	-15.571	18.629
7	15.207	34.928	**25**	45.617	-18.029	**43**	-21.375	-34.385	**61**	-28.823	11.610
8	57.806	25.570	**26**	33.317	-15.873	**44**	-9.896	-20.907	**62**	-39.169	16.442
9	36.930	22.191	**27**	14.705	-11.003	**45**	-17.660	-22.011	**63**	-29.618	25.641
10	26.158	21.465	**28**	16.208	-22.206	**46**	-30.982	-20.231	**64**	-11.293	31.465
11	11.676	21.531	**29**	4.540	-23.467	**47**	-47.917	-23.374	**65**	-27.496	40.753
12	3.615	24.247	**30**	56.983	-35.982	**48**	-54.667	-27.759	**66**	-42.338	37.879
13	44.746	5.035	**31**	38.695	-30.531	**49**	-2.614	-15.641	**67**	-57.622	30.862
14	30.054	7.361	**32**	24.473	-36.881	**50**	-48.234	-11.071	**68**	-9.501	51.605
15	18.791	10.272	**33**	13.829	-35.359	**51**	-5.466	-6.682	**69**	-24.369	54.563
16	10.809	12.377	**34**	45.139	-46.618	**52**	-16.420	-4.635	**70**	-46.127	52.126
17	6.875	10.035	**35**	24.375	-55.247	**53**	-24.660	-7.091			
18	53.553	-3.738	**36**	7.556	-56.978	**54**	-35.912	-1.146			

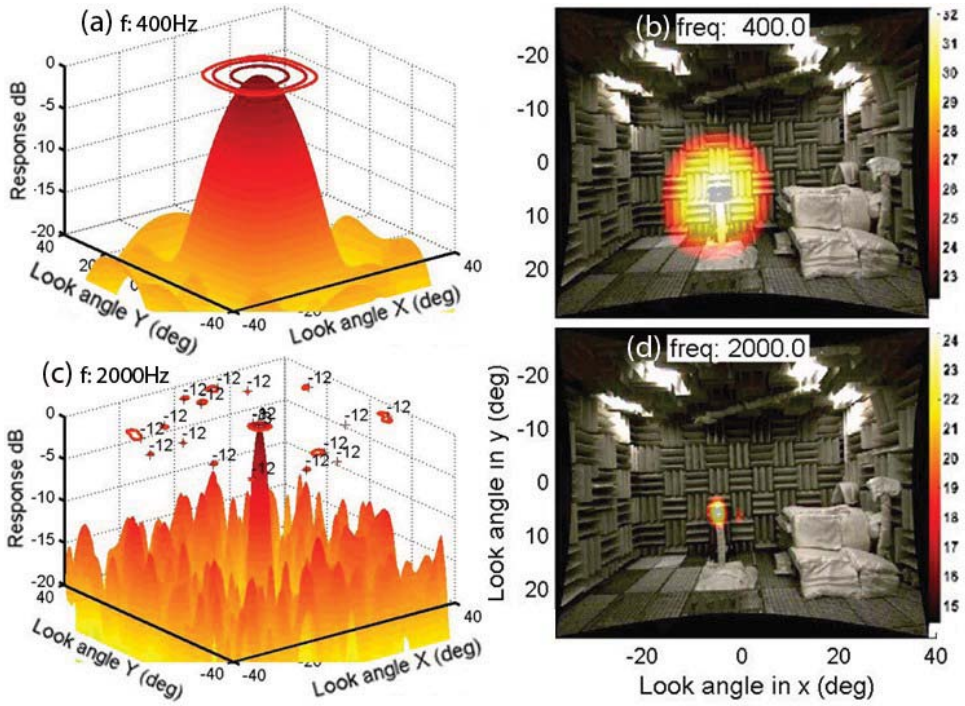

Fig. 4 *Comparison between calculated and measured point spread function (psf) at two indicated frequencies. Calculations are for a source at x=y=0°, and z = 740 inches.*

Additional precautions had to be taken to protect the cameras and microphone sensors from exposure to moisture during long outdoor stay, and from steam generated during launch. The array chamber was continuously purged with low pressure Nitrogen (Fig 1d shows the nitrogen skids). When nitrogen was not available, a dehumidifier was placed inside the chamber. However, the most useful protective elements were the thin windows made of Mylar® film that were glued in front of each microphone (Fig 3b). In addition to providing protection from rain, the Mylar® films blocked the storm of sand and other debris, created during the launch, from impinging on the sensors. All sensors survived multiple rainstorms and the Antares launch, proving effectiveness of the protective devices. The particular Mylar® film was chosen after a test of transmission loss in an anechoic chamber where the loss was measured to be less than 0.1dB.

An 80 channel, 24-bit PXI system was used for simultaneous acquisition of the microphone and accelerometer signals. In addition, a time pulse at the ignition of the Antares engines (t = 0) was recorded to synchronize the microphone signals with the launch events. Each microphone channel was simultaneously sampled at 20480 samples/s; providing a usable bandwidth of greater than 8 kHz. Personal computers using all solid-state devices were used for data and image acquisitions. The amplifiers, data acquisition system and the computers were kept in a concrete building next to pad 0A. For the Ames hybrid rocket test they were kept in a separate enclosure behind the array box. The personal computers interfacing with the data and video acquisition systems were accessed over a local network from a remote station. The data acquisition was started manually at t-30s and lasted for 60s.

III. PHASED ARRAY DATA PROCESSING

IIIa. Conventional beamforming (CB):

To create maps of the noise sources first, the region where such sources are expected to be present is divided into a set of grid points. Typically a planar phased array is somewhat insensitive in the depth direction (i.e. along the normal to the array plane); therefore a two-dimensional set of grid points (also called interrogation points) is setup. Let j =1, 2, 3…N be the interrogation points, and m = 1, 2, …M be indices for microphones. The radial distance r_{jm}, from an interrogation point to an individual microphone, determines the phase shift and the relative amplitude measured by the microphone. The steering vector is a column matrix defined to incorporate these properties:

$$w_{j,m} = \frac{r_{jm}}{r_{jc}}\, e^{-ik\, r_{jm}} \qquad \textbf{(2)}$$

Here r_{jc} is the distance of each interrogation point to the center of the array. Note that: $\boldsymbol{w}_j^{\dagger}\boldsymbol{w}_j = 1$. The above equation is valid if the noise source radiates as a monopole. This basic assumption of the beamforming process has been under scrutiny for the entire history of the phased- array technology. The justification has been the little change in the beam-formed map obtained by assuming other type of sources. Additionally, a lift-off environment is made of a variety of sources, some of which are distributed and some of which are compact, whose pole types may not be known a priori. The possibility of making a significant error is minimized by assuming that the noise sources are made up of an agglomeration of many monopoles.

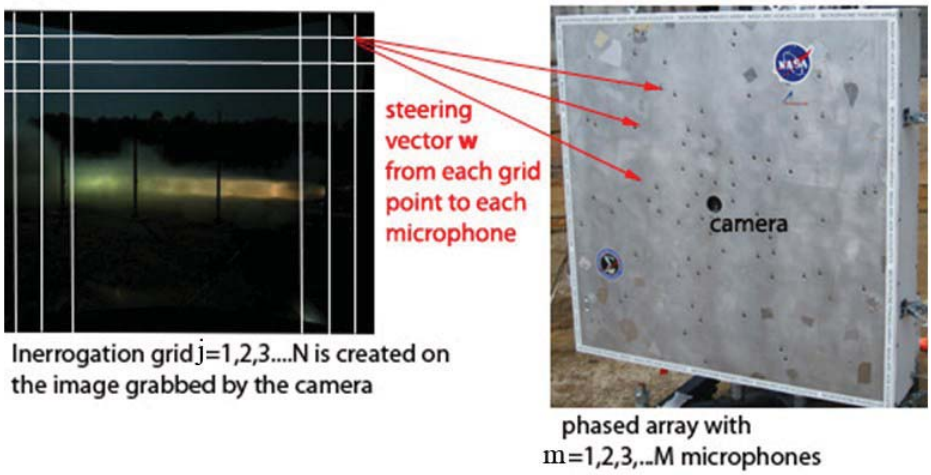

Fig. 5 *Schematic of beamforming process.*

The time traces of pressure fluctuations from individual microphones are Fourier transformed to obtain individual spectra $P_m(f)$. The phase and amplitude relations between every pair of microphones are calculated and stored in a cross-spectral matrix **G**. Every element of the cross-spectral matrix (CSM) is calculated as:

$$G_{mm/} = \langle P_m{}^* \, P_{m/} \rangle \qquad \textbf{(3)}$$

Typically the Fourier transform is performed over multiple overlapping blocks of data which are then multiplied using the above equation and finally averaged to obtain individual elements of the CSM. The diagonal elements of the CSM G_{11}, G_{22}, G_{33}, etc. contain the auto-spectra which are contaminated by various spurious noise sources, such as electronic noise and wind generated noise. Zeroing out the diagonal elements improves the beamformed map [9].

The summing of the microphone signals, i.e. the elements of cross-spectral matrices, needs to be preceded by a phase adjustment. These two steps are combined in a matrix manipulation which leads to the conventional beamform map:

$$b_{jj}(f) = w_{j,m}{}^{\dagger} G_{m,m/} \, w_{j,m/} \qquad \textbf{(4)}$$

To improve resolution, a linearly increasing weight S_m based on the radial location R_m of the microphone was used with the conventional beamforming process [10]:

$$S_m = S_1 + (1 - W_1) R_m / R_0 \qquad \textbf{(5)}$$

The two constant S_1 and W_1 were set to 0.1; R_0 represented radius of the outermost microphone. The row matrix S containing weight factors were used in the following fashion.

$$b_{jj}(f) = \frac{w_{j,m}{}^{\dagger} (SGS^T) \, w_{j,m/}}{(\sum_m S_m)^2} \qquad \textbf{(6)}$$

It is worth mentioning here that the noise source results presented in this paper are subjected to the inherent assumptions of the conventional beamforming process: that the complex sources can be modeled as sum of many monopoles, and sound propagation is strictly linear.

IIIb. Direct Spectral Estimate – Spectral Element Method (SEM) [11]:

A well-known fact about conventional beamforming process is that it causes excessive smearing of the noise sources at the low frequency end, and produces pseudo-sources (side lobes) at the high frequency end. This is due to the inherent instrument function (also called the point-spread-function) of the phased array. The instrument function, however, can be calculated if the sound radiation character of the individual sources is known *a priori*. The discussion above assumes that the sound sources are made of uncorrelated monopoles, which is also followed in the SEM method. However, instead of making phase adjustment via Eq 4 above, the direct spectral method attempts to find the strength of the monopoles directly from the measured cross-spectral matrix G. To this end the noise source region is divided into N_s interrogation

points (also called grid points) and a model cross-spectrum between two microphones m and m/ is calculated as following. The unknowns in the model are the strengths of the monopole sources α_j^2 at each of the interrogation point j = 1, 2 … N_s.

$$G_{mm/}^{mod} = \sum_{j=1}^{N} w_{j,m}\alpha_j^2 w_{j,m/}^{*} = \sum_{j=1}^{N} \left(\frac{r_{jm}}{r_{jc}}\, e^{-ik\, r_{jm}}\right) \alpha_j^2 \left(\frac{r_{jm/}}{r_{jc}}\, e^{-ik\, r_{jm/}}\right)^{*} \qquad \textbf{(7)}$$

The positive values of α_j^2 assure elimination of the unphysical negative sources. In the method proposed by Blacondon & Élias [11] the source distribution is determined via minimization of error between the measured and the modeled cross-spectra.

$$E(\alpha_j, f) = \sum_{m,m/=1}^{J} \left| G_{mm/} - \sum_{j=1}^{N} w_{j,m}\alpha_j^2 w_{j,m/}^{*} \right|^2 \qquad \textbf{(8)}$$

Note that the measured cross-spectral matrix G contains (M^2-M)/2 number of independent, non-diagonal, complex values when the diagonal terms are deleted. Counting the imaginary and the real numbers separately, the total number of independent variables to be minimized becomes *J*, which is used in Eq 7 above.

$$J = M^2\text{-}M \qquad \textbf{(9)}$$

Similar to a procedure followed by Casalino et al [12], the calculations were carried out in Matlab® using routine *lsqnonneg* that uses a non-negative least square process. Various applications involving plume acoustics have used the SEM method in the past [5, 13].

IIIc. Modified SEM

The modeled cross-spectrum of Eq 7 does not account for an important property of distributed noise sources, namely a loss in coherence between microphone pairs. The monopole model used for the phased array processing assumes a coherence of unity among every microphone pairs. However, the measured data show a progressive lowering in coherence as the separation between the microphones is increased [2]. The coherence levels drop precipitously with frequency; also the more distributed a source, the weaker is the coherence. While sound from a compact point source, such as a single speaker produces coherence level of unity over microphones placed at wide angular separations, a distributed source such as a jet or a plume creates sound that quickly becomes uncorrelated within a small angular separation. This fundamental property was discussed in detail by Tam et al [14]. The coherence between every pair of microphones m and m/ can be calculated easily as following:

$$\Gamma_{mm/}^2 = \frac{G_{mm/}}{|P_m|\left|P_{m/}\right|} \qquad \textbf{(10)}$$

The modified SEM used in the present paper simply uses a model cross-spectrum whose magnitude is reduced by the measured coherence:

$$G_{mm/}^{mod} = \Gamma_{mm/} \sum_{j=1}^{N} w_{j,m}\alpha_j^2 w_{j,m/}^{*} \quad \textbf{(11)}$$

$$E(\alpha_j, f) = \sum_{m,m/=1}^{J} \left| G_{mm/} - \Gamma_{mm/} \sum_{j=1}^{N} w_{j,m}\alpha_j^2 w_{j,m/}^{*} \right|^2 \qquad \textbf{(12)}$$

Since Eq 11 is a more realistic model of the measured cross-spectrum, the least square method is found to converge easily with less iteration. However, for higher frequencies, when the coherence levels become very poor for a majority of the microphone pairs, the difficulty in attaining a converged solution returns. A different array pattern is warranted to resolve higher frequencies.

IV. MATLAB® IMPLEMENTATION:

The above beamforming schemes were implemented in the commercially available Matlab® platform. A personal computer with a six-core processor was used along with the Matlab® Distributed Computing Toolbox. Once the cross-spectral matrix (Eq 3) was calculated the rest of the beamforming operation for both conventional and SEM methods happened fairly quickly (few seconds for each frequency bin). Depending on the time duration of the microphone signals, the CSM calculation took between one-half to three minutes.

To facilitate direct identification of the noise sources, the interrogation grid was created over a photograph of the region of interest captured via either the visible band or the infra-red band video camera mounted at the center of the array. When the noise source was stationary, a single frame of the captured video was sufficient for further processing. The following section describes the process applied to the stationary sources. The additional steps needed for the moving launch vehicle are described later in section VII. The first processing step after selecting the frame was to perform a correction for barrel distortion due to the fish-eye lens used with the camera using the following relation.

$$s = r + \alpha r^3 \qquad \textbf{(13)}$$

Here α is the correction factor, r: radius of each pixel from the center of the image, and s: corrected radius. The correction factor, a fixed number for a given lens, was established by trial and error. In the next step the photographed region was divided into a uniformly spaced grid. To select the number of grid points, Rayleigh criterion was applied to the highest frequency of interest (Eq 1). Typically the grid spacing obtained using the Rayleigh criterion was refined by a factor between 6 and 20; the higher the factor the slower the processing.

The cross-spectral matrix (CSM) of Eq 3 was the first step in data processing. Once computed, the CSM can be used with any number of beamforming methods without a need for recalculation. In the next step the conventional beamforming was performed (Eq 4), followed by a superposition of the beamformed colored maps on a video frame from either the visible band or the IR-band camera.

Correct registration of the beamformed map and the video frames required a calibration process. The look-angle of the video camera changed slightly every time the array was rebuilt. To correct for such a small but important change, a speaker was placed at various locations in the camera field of view, and the video image was rotated in pitch, yaw and/or roll directions for correct superposition of the beamformed maps. The alignment error found from this calibration process was used to process test data. This calibration step was applied to both the visible and thermal wavelength cameras.

Implementation of SEM typically required fewer grid points. Papamoschou [13] suggested that the total number of grid points be equal to the total number of unknowns J (Eq 9). However larger numbers of grid points were found to provide similar results but required longer computing time. To limit the computing time to a reasonable duration, the maximum number of iterations in *lsqnonneg* routine was limited to 500.

One difficulty with SEM was the excessive localization of a distributed source. A speaker source became localized to a single grid point, which provided the impression of a highly effective scheme. However, the noise sources in a free plume became localized to a set of discrete points, which was unphysical. The localization was so sharp that single, discrete grid points were identified as sources. To make such points clearly visible, the Savitzky-Golay polynomial smoothing filter was used to smear the discrete point sources. The smeared map made the discrete points to appear more distributed. Matlab® routine *sgolayfilt* was used for this purpose.

V. RESULTS FROM THE STATIC TEST FIRING OF SMALL SCALE HYBRID ROCKET ENGINES

Figure 6 shows a photograph of the array chamber at the NASA Ames hybrid combustion facility. The phased array program took advantage of a series of tests conducted to develop paraffin-N_2O hybrid rocket engines in the 25,000 lbf thrust range [15]. Participation in this series of tests helped to improve familiarity with the newly built array, to fix hardware and software related problems, and to provide an in-house preparation stage before the remote-site launch related activities. Multiple problems related to exposure to rainstorms and the high vibration levels of a rocket firing were observed and corrected. The test stand was built on a concrete and steel floor which acted as acoustic reflectors. The top halves of each orange-red noise map of Fig 7 are along the actual plume (the actual plumes are not shown as the photographs are from

just before firing) and are the true noise sources. The bottom halves of the orange-red noise maps are reflections off the floor. The phased array resolved sources of both direct and reflected sound waves that reached its sensors, however; the close proximity of the plume to the ground surface did not allow for any separation between the actual and the reflected sources. Another interesting observation is the unrealistic noise maps obtained using SEM (modified SEM for the present case). The SEM scheme was found to be useful for compact sources but not so much for distributed sources. Despite using the smoothing filters on the noise maps, the distributed noise source of the long plume was fragmented into multiple spots as seen in Figs 7(c) and 7(d). The scenario was analogous to earlier results obtained via CLEAN-SC from a different rocket plume where the spatially correlated regions of a distributed source were similarly replaced by discrete points [1]. Although the two methods differ in implementation, but the central difficulty in treating a correlated noise source seems to be similar.

Fig. 6 *The large array setup at NASA Ames hybrid combustion facility.*

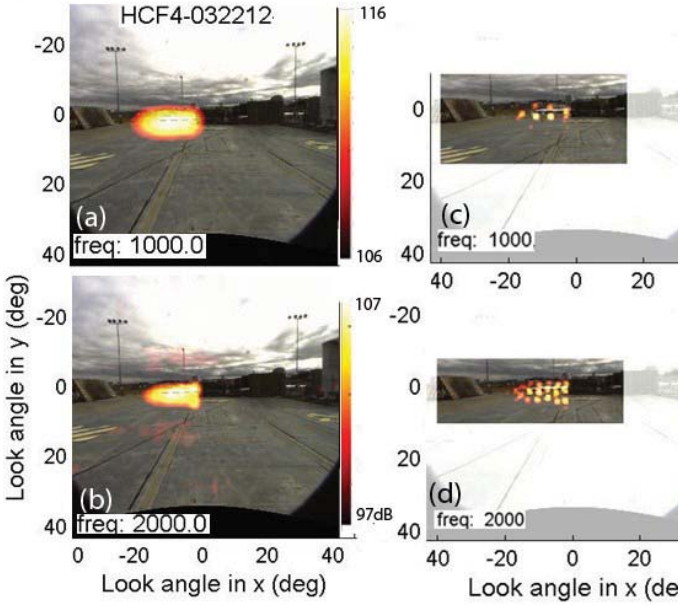

Fig. 7 *Noise maps from a hybrid rocket test firing; (a), (b) conventional beamform; (c), (d) modified-SEM beamform.*

VI. RESULTS FROM FULL-SCALE STATIC-FIRE TEST OF ANTARES FIRST STAGE ENGINES

After the initial testing at NASA Ames Research Center, the phased array was dismantled and shipped to NASA Wallops Flight Facility where it was re-assembled. After connecting all sensors, cameras and cable bundles, performing another set of microphone calibration, and an overall system check, the array structure was lifted and secured inside the basket of a large scissor lift. The scissor lift was driven to a parking lot close to launch pad 0A (Fig 1d). The location for the array was decided after much deliberation on accessibility, cost of operation, and ease of approval from Orbital Sciences Corporation and Mid-Atlantic Regional Spaceport. The participation was subjected to a non-interference criterion, where the operation of the phased array could not interfere with the vehicle and launch pad preparation activities. Because a phased array identifies the locations and levels of sources of sound waves propagating towards its direction, ideally the array would be located near the launch vehicle; however, that would have violated the non-interference criteria. The best compromise was found to be a location outside a fence surrounding the immediate hazard zone, in the parking lot of an adjacent building (z40) that was used for various preparatory activities. The scissor lift stood on

outriggers, and the lift basket carrying the array chamber was hoisted 40 feet above ground. The elevation provided a clear view of the launch pad, above various obstacles, and ultimately identified noise sources radiating upwards. To secure the lift basket from excessive sway in high winds and from the high vibratory loads during launch, four guy wires were tied between the corners of the lift basket and ground. The guy wires helped to reduce the vibration which was still very high. The specification for the thermal imaging camera was for a maximum level of 2g. The camera failed during this test and did not produce any images. However rest of the equipment survived and provided good data. Another expected consequence of heavy shaking was phase jitter and a loss of coherence among microphones. However, the burn lasted for a long time which allowed for sufficient averaging to reduce the net influence.

The static fire test ("7K -TEST") took place on February 22nd, 2013. The vehicle configuration for the static-fire test can be seen in Fig 1(c). Only the first stage engines, the cryogenic propellant tanks and the bottom part of TEL were erected. The engines were mounted on the top of the flame duct with a special test mount for the long, 29-second duration test. Water was injected inside the flame duct as well as on the top of the deflector. Figure 1(c) shows the hot plume and steam emerging from the duct exit. Traces of the hot plume are also visible through the gaps in the engine mount. The phased array is barely visible at the right edge of this figure. The engine thrust variation is shown in Fig 8(b). The engines were also gimbaled over a wide angular range during the burn. The acoustic signature mostly followed the thrust pattern with minor differences from the additional variables. Figure 9 shows the noise maps at two different frequencies calculated via beamforming. One frame from the visible wavelength camera was used for the background photograph. Note that the conventional maps show the top 10dB range of source distribution while the SEM maps show 20dB range. Data from the peak 14.5s duration shown in Fig 8(a) was used to calculate the noise maps. Interestingly the duct exit was found to be the most prominent noise source at all frequencies. The higher dynamic range of the SEM maps show that the engine mount, at the bottom of the vehicle was also a source, albeit weaker by 16dB.

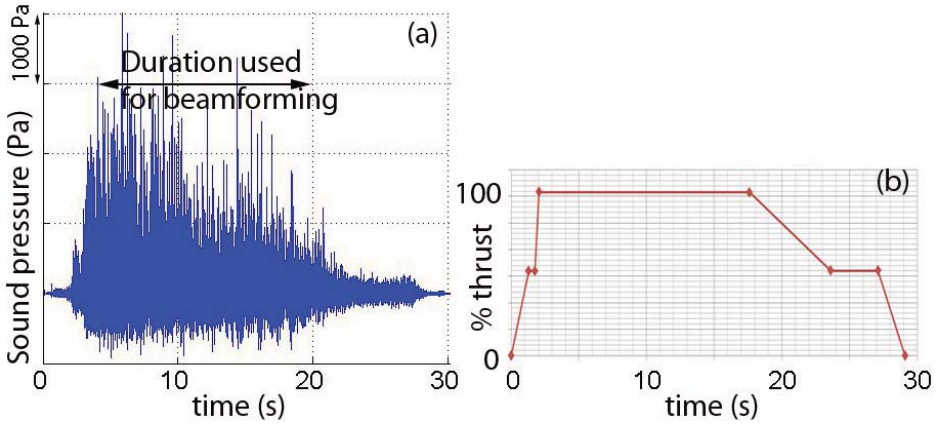

Fig. *8* *(a) Time trace of the pressure fluctuations from one microphone, and (b) Engine thrust variation from the static fire test of the Antares Engines.*

That the duct exit is the overwhelmingly loud noise source, instead of the plume itself, is an interesting observation. The hot gases from the engine plume shot out through the duct. The traditional modeling expectation [3] is of a long distributed source along the plume path. The beamform maps revealed a very different scenario. It is believed that the large amount of water sprayed into the flame duct quenched the plume and significantly reduced its ability to generate noise. It is the noise generated inside the closed duct, due to impingement on the deflector, and due to the general turbulent mixing, that ultimately radiated out through the exit. The noise maps of Fig 9 also indicate a path to further attenuate the acoustic level on engine components during

a static-fire test. Such attenuation can be obtained simply by extending the length of the duct to make the exit further away from the vehicle.

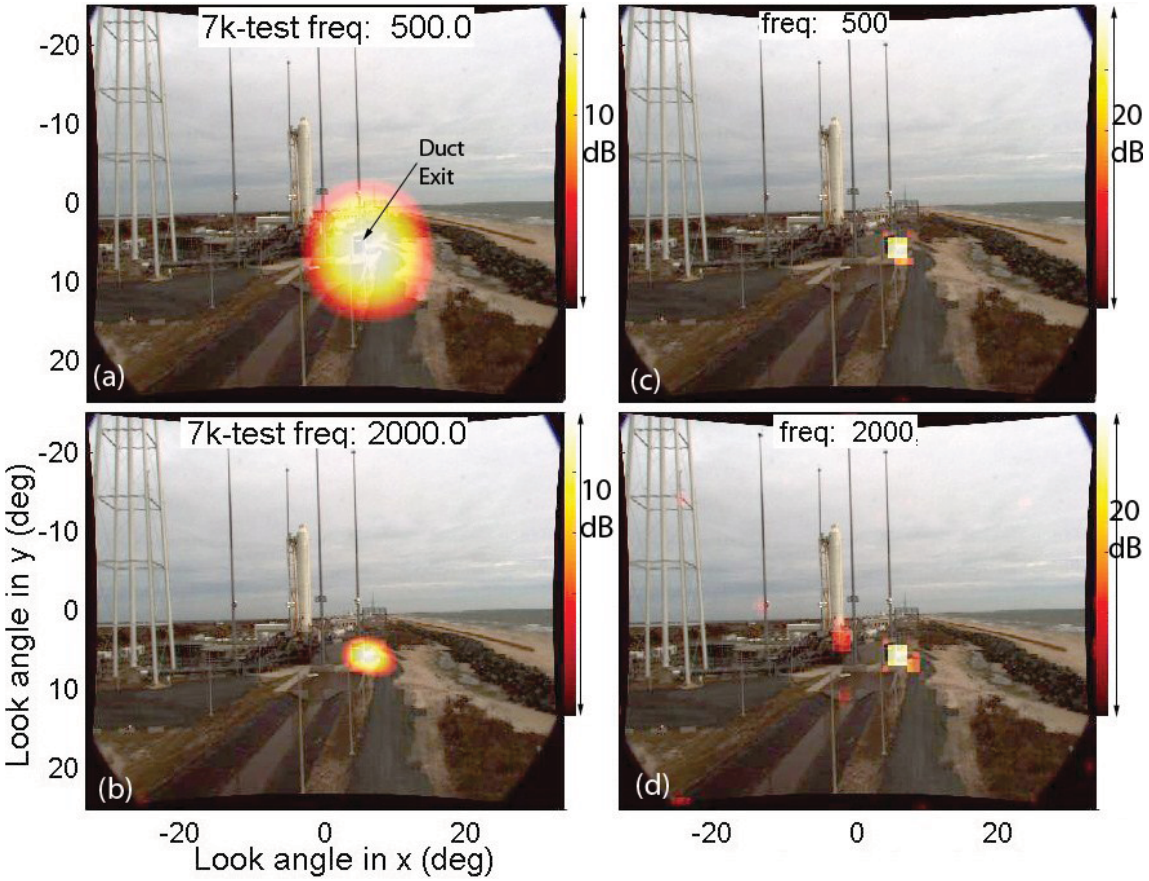

Fig. 9 *Noise sources during engine hot-fire test at indicated frequencies calculated via (a), (b) conventional beamform and; (c), (d) modified SEM. Note different plot range for the color scales.*

VII. RESULTS FROM ANTARES A-ONE LAUNCH

The array was re-deployed at the same parking lot, and about 400 feet away from the vehicle for the maiden launch of Antares (Fig 1a, 1b, 1d). The launch took place on April 21st, 2013. In this installation, only a lighter weight scissor lift was available, necessitating use of additional guy-wires (eight instead of four in the static-fire test) to steady the array. Also an improved vibration isolation mount allowed the thermal camera to provide video footage for the first 10s after ignition. Unfortunately, six of the seventy microphone channels were inadvertently turned off, effectively making a 64 microphone array. Nevertheless, the data provided good insights into the acoustic sources. The “speaker calibration” process to determine the look angle of the cameras was performed the night before launch by placing a loudspeaker at a couple of different locations around the pad. The beamformed maps from this speaker when superimposed on a frame of the video footage provided the angular differences between the array coordinates and the camera “look angle.” This correction was established for both the visible and the thermal imaging cameras.

The Antares vehicle accelerated somewhat slowly. Two seconds after the first stage’s twin AJ26 engines were ignited the rocket lifted off the pad (Fig 10a). Eight seconds later, the rocket was traveling at 65 km/h and was just 70 meters off the pad. The slow motion of the vehicle made any correction for Doppler shift unnecessary in the beamforming calculations. Just before ignition the vehicle was released from the TEL which tilted back to avoid re-contact. In addition,

the vehicle was pitched away from the TEL early in the liftoff to provide additional margin (Fig 10b). This “TEL avoidance maneuver” significantly affected the noise source distribution. All three water injection systems for acoustic attenuation (described earlier) were used during the launch.

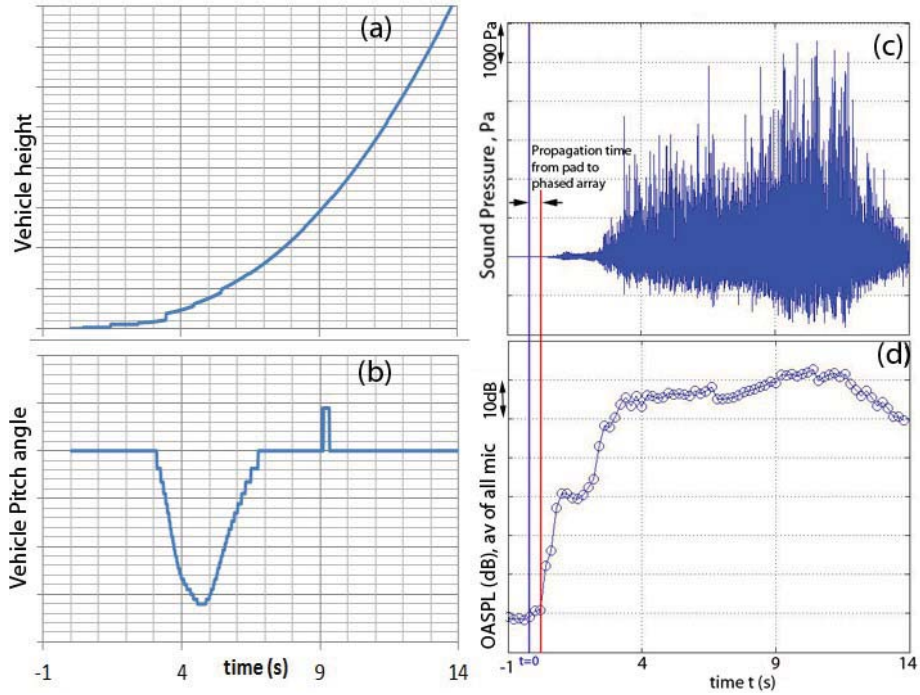

Fig. 10 (a) *Height and (b) tilt angle of Antares during A-one launch; (c) time-trace of noise signal from one microphone in the phased array; (d) time variation of overall sound pressure level at the phased array.*

The noise sources during a launch are much more time dependent than during a static fire. For correct time registration between the beamformed maps and the launch events the propagation delay of the sound waves from the pad to the face of the array needed to be accounted for. This was simple to determine from the known distance of the array and the ambient speed of sound. Figure 10(c, d) shows the propagation delay on the time trace of the pressure fluctuations measured from a microphone. A launch site next to the ocean is never a quiet place. The wind noise and the noise from various bleed operations were around 90dB before engine ignition. The ignition and powering-up of the engines created progressively higher levels. However, the loudest level of >150dB was measured when the vehicle was ~120 meters above the launch pad, and the entire plume emerged out of the flame duct.

To determine the time evolution of the noise sources, the microphone signals were divided into 0.2s-long segments and the beamforming process was applied to each segment. The beamformed maps were superimposed on individual frames from the thermal imaging camera. Figure 11 shows the evolution of the noise sources at different time intervals. The right column of Fig 11 is from selected frames of a high speed camera (courtesy of NASA KSC imaging group) that provided an excellent view of the launch events. Before embarking upon a discussion of the noise maps some elaboration of the individual images shown in the left column of Fig 11 is warranted.

Each image in the left column of Fig 11 is a composite of three images: (a) a beamformed noise map whose levels are shown in the color scale; (b) the bottom part of a temperature map from just before the ignition; and (c) the top part of the temperature map at the time instance marked on the figure. The merging of the latter two was necessary to provide a definition of the pad which was obscured in the actual footage. In Fig 11(a), the thermal image

of the Antares was split by the central dark zone that corresponded to the cold LOX tank. The bottom RP1 tank and the top part of the vehicle were warmer and fell within the grey scale of the image. As the launch events progressed the acoustic levels became louder and the camera started to shake. This produced increasingly blurred image of the Antares vehicle which is barely visible in Fig 11(d) onwards. However, these figures correctly show the locations of the high temperature plume from the engine exhaust. The color scale for the noise maps show dB level calculated from an 80Hz wide band centered at 2 kHz. The 10dB plot range was auto-scaled for each of the maps.

Figure 11(a) was from just after ignition when the engine was at partial power, and the hot plume was visible through the openings of the launch mount. These openings allowed for the emergence of the sound waves and were the primary noise source at the beginning. The ground reflection of the primary source was also seen as a second source by the array. The reflected source persisted in Fig 11(b).

Some amount of steam and water from inside the duct started to emerge starting at the time of ignition. However, the duct exhaust did not become a prominent source until the engine came to nearly full power and hot gases began to emerge (Fig 11c). At this point both the inlet and the exit of the duct were noise sources. The next three figures 11 (d) - (f) show a problematic spread of the noise sources from the duct ends to the top of the pad. The cause was a spilling of the hot plumes from the Antares engines over the pad. An examination of the vehicle alignment with the nearby lightning protection tower in the right image of Fig 11(d) show the tilting of the vehicle as a part of the “TEL avoidance maneuver.” The thermal camera images show white patches on the pad indicative of high temperature gas. The combination of tilting of the vehicle and drift towards the east (ocean-side) caused the hot plume to spill out of the duct inlet and spread over the pad. Figures 11(e) and 11(f) show an increasing amount of spill and spread of hot gas all over the pad. This condition was created by a relatively late start of the on-deck “rainbird” system. Even the earlier-start rainbirds did not come to full flow rate until the vehicle was elevated 40 feet above the pad. In the right side images of Fig 11(d) – (f), from the visible wavelength camera, the orange glow can be identified with the hot plume, and the white glow with steam. Very little steam is found to rise from the top of the pad during the early part of lift-off. The plots of Fig 11 clearly show a need for an earlier start of the rainbirds. This will be implemented in future Antares launches. The early start will quench the plume and the impingement zones, resulting in less damage and a lower acoustic level.

As the launch progressed part of the plume emerged from the duct, and the beamformed maps correctly identified the plume itself as the dominant source. Figures 11(g) and 11(h) show sufficient quenching by the rainbird system which reduced the extent of the noise source on the top of the concrete pad, leaving the exposed plume as the primary source. A small amount of ground reflection is also visible in the noise map. Figure 11 shows plots from a few selected time segments. A movie using all time instances provided some more details; although the central conclusions were the same.

Beyond the last time frame shown in Fig 11, the plume and the noise maps simply became longer until most of the plume crossed the upper edge of the camera images; the overall acoustic level started to fall due to an increased forward velocity of the launch vehicle. SEM beamformed maps were once again found to discretize the distributed noise sources on the long plume. Due to the shorter time duration, phase jitter from the shaking of the array chamber, and the inadvertent power loss of 6 microphones, SEM maps showed increased side-lobes in plots covering a wider dB range. Since no new insights were gained via SEM calculations such maps are not shown here.

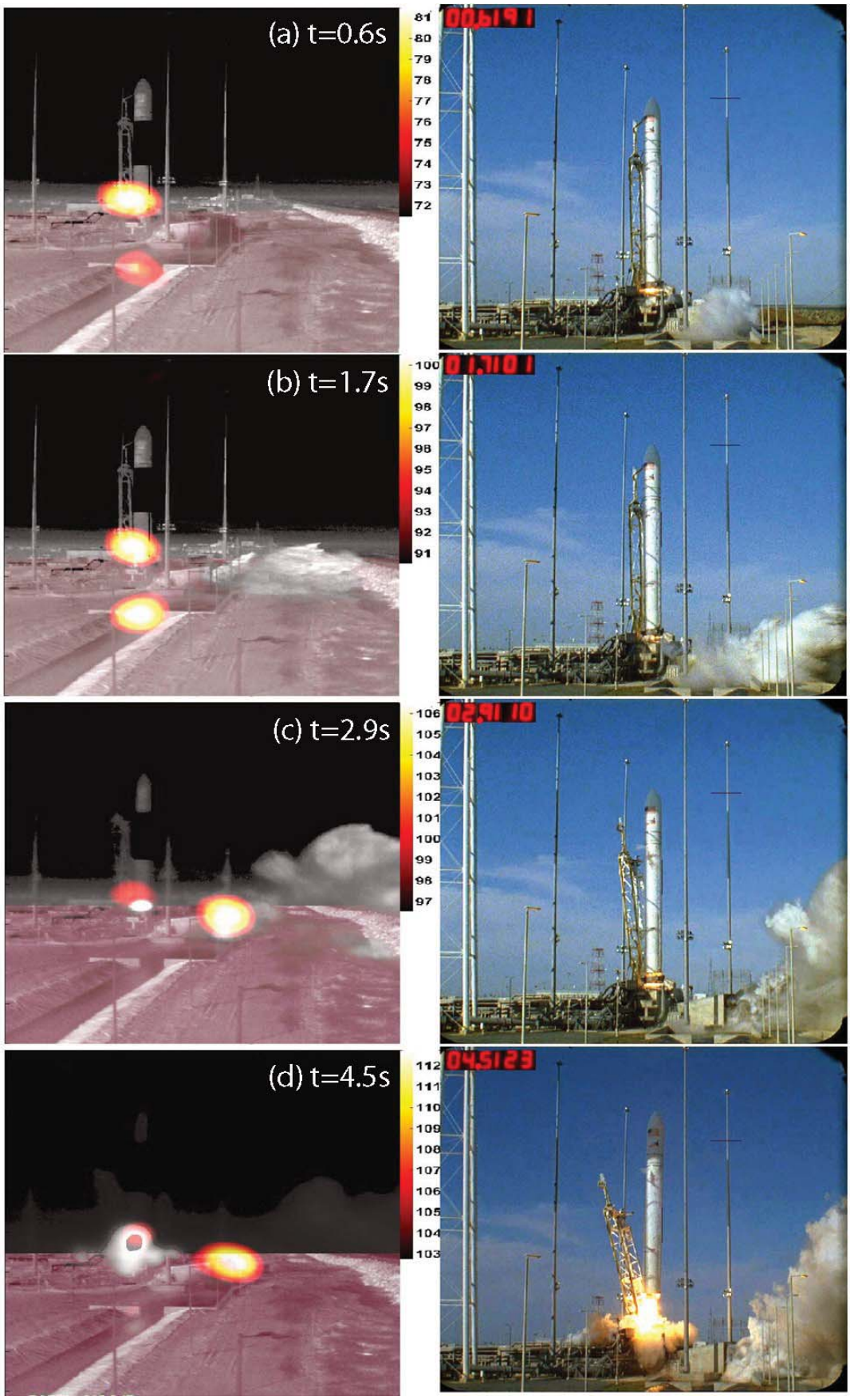

Fig. 11
Contd.

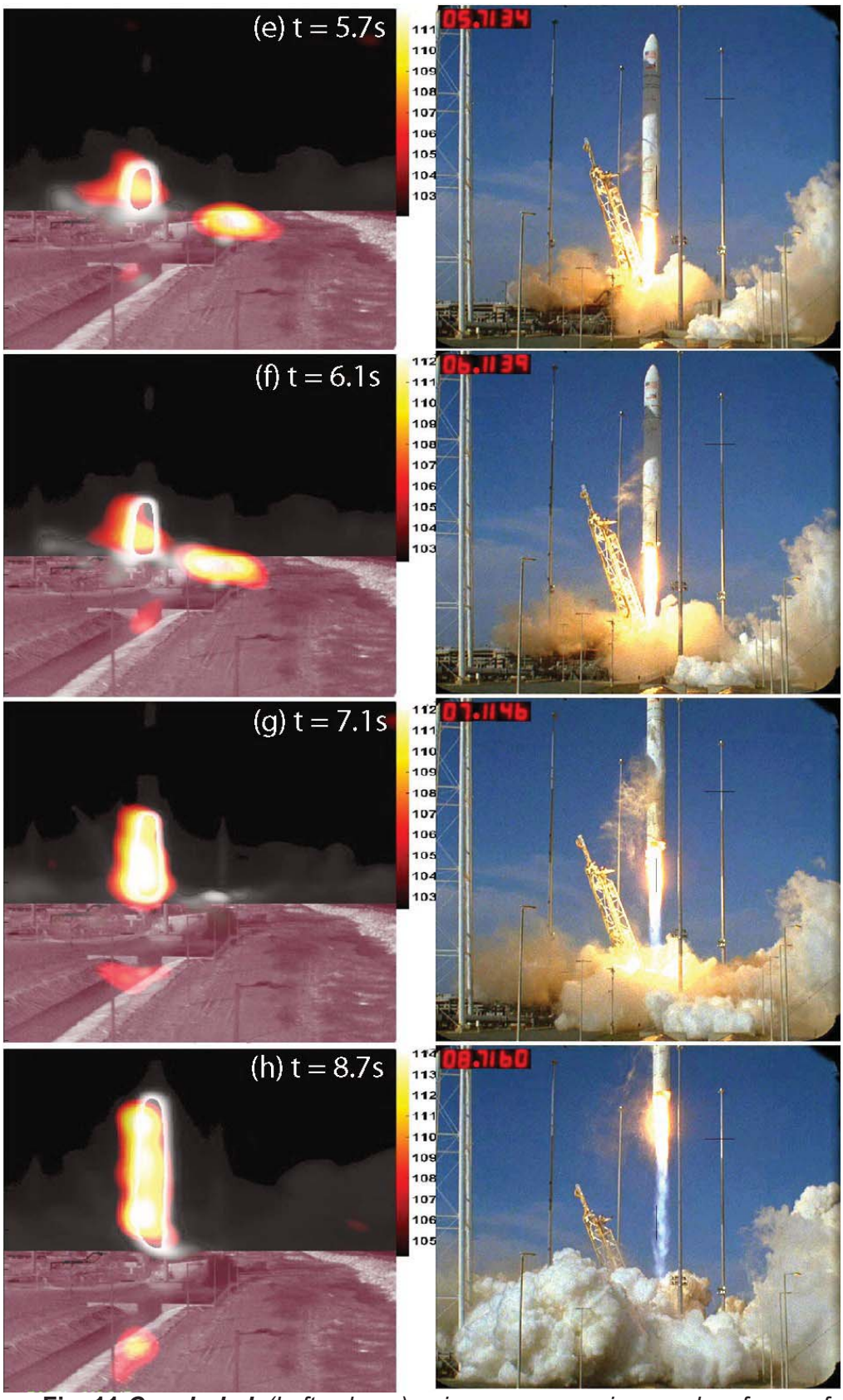

Fig. 11 ***Concluded.*** *(Left column) noise maps superimposed on frames from IR camera, conventional beamform at 2 kHz; (right) corresponding frames from a high-speed camera.*

VIII. CONCLUSIONS

The evolution of the acoustic sources during static-fire engine tests and a rocket launch was measured using a microphone phased array. Although the present demonstration was performed on the Antares rocket, but the technology developed for this work is applicable to any launch vehicle. The goal of the work was to advance the phased-array technology for launch vehicle applications. The actual noise sources are expected to vary for different launch pads and rocket vehicles. The use of phased-array technology, as demonstrated in this paper, may lead to improvement of the acoustic suppression systems and lowering of the vibro-acoustics load.

A 10-foot by 10-foot, large yet portable, phased array was built for use at the launch pads of rocket vehicles. The array used 70 condenser microphones, and two video cameras that operated in the visible and long infra-red wavelengths. The infra-red camera was used to visualize the location of the plume and various impingement zones on the launch pad. The microphone pattern was designed for optimal resolution in the relatively low (400Hz to 2000Hz) frequency range. At first, the array was tested during the static firings of a small scale hybrid engine at NASA Ames. It was then shipped to NASA Wallops for set up at launch pad 0A. There the array was used during a static test firing of the engines of the Orbital Sciences' Antares rocket, and again during the first launch of Antares. It was placed 400-feet away from the pad, and was hoisted on a scissor lift 40-feet above the ground to obtain a good view of the top of the launch pad. Data collected from these efforts provided remarkable insight into acoustic sources in a full-scale static-fire, and a launch, not previously available.

For the static fire test the twin LOX-RP1 liquid engines of the Antares vehicle were mounted above the flame duct that included a deflector and a water injection system. During the static-fire test it was found that the duct exit was the primary noise source, while the nozzle exit and the engine mount were weaker, secondary sources. Unlike most of the models of launch acoustics, such as NASA SP 8072 [3] the plume that emerged out of the duct was not found to be a source. Fundamentally, the noise generated inside the duct from impingement and turning of the plume, and from general turbulent mixing, emerged from the duct exit. The plume was sufficiently cooled and slowed inside the duct, and did not radiate significantly as it emerged.

The noise sources during lift-off of Antares vehicle was found to vary with time. During engine ignition the launch mount was the source. As the engine came to full power, and hot plume came out of the duct, the exit face of the duct was found to be the most prominent source. Effective cooling by duct water limited the extent of this source and kept the acoustic levels to a reasonable value. As Antares started to elevate, it tilted east (towards the ocean) and drifted away from the duct hole as a part of the maneuver to avoid contact with the service mast. This caused the hot plume to spread over the pad. A large region on the top of the pad became a loud noise source. Further elevation of the vehicle, and the start of the rainbirds, reduced the extent of the source. As more and more plume emerged out of the hole, the plume itself became the noise source – duct exhaust was no longer a source. Cooling by the rainbirds attenuated sources on the top of the deck. The phased array also identified ground reflection of the primary sources at ignition and again when the long plume emerged out of the duct. Based on the insights gained from the phased array effort the rainbird timing will be changed for an earlier start for the next launch of the Antares vehicle.

References:

[1] Panda, J. & Mosher, R. "Use of a Microphone Phased array to Determine Noise Sources in a Rocket Plume," *49th Aerospace Sciences Meeting*, AIAA paper 2011-974, 2011.

[2] Panda, J. & Mosher, R., "Microphone Phased Array to Identify Liftoff Noise Sources in Model-Scale Tests," Journal *of Spacecraft and Rockets*, Vol. 50, No. 5, Sept-Oct 2013. DOI: 10.2514/1.A32433

[3] Eldred, K. M. & Jones, G. W., Jr., “Acoustic load generated by the propulsion system,” NASA SP-8072, 1971.
[4] Plotkin, K. J., Sutherland, L. C., & Vu, B. “Lift-Off Acoustics Predictions for the Ares I Launch Pad,” *15th AIAA/CEAS Aeroacoustics conference*, AIAA paper 2009-3163, Miami, Fl, 2009.
[5] Gély, D., Elias, G., Bresson, C., Foulon, H., Radulovic, S, 2000 “Reduction of supersonic jet noise. Application to the Ariane 5 launch vehicle,” *6th AIAA/CEAS Aeracoustics Conference*, AIAA paper 2000-2026, 2000.
[6] Fukuda, K., Tsutsumi, S., Fujii, K., Ui, K., Ishii, T., Oimuna, H., Kazawa, J., Minesugi, K., “Acoustic Measurement and Prediction of Solid Rockets in Static Firing Tests,” AIAA paper 2009-3368, 2009.
[7] Brehm, C., Sozer, E., Moini-Yekta, S., Housman, J. A., Barad, M. F., Kiris, C. C., Vu, B. T. & Parlier, C. R., “Computational Prediction of Pressure Environment in the Flame Trench,” AIAA paper no 2013-2538.
[8] Underbrink, J. R. “Aeroacoustics Phased array Testing in Low Speed Wind Tunnels,” in *Aeroacoustics Measurements, Springer, Ed. Thomas J. Mueller,* pp. 98- 217, 2001,.
[9] Daugherty, R. P. “Beamforming in Acoustic Testing,” in *Aeroacoustics Measurements, Springer, Ed. Thomas J. Mueller,* pp. 62-97, 2001
[10] Brooks, T. F., & Humphreys, Jr., W. M., “A Deconvolution Approach for the Mapping of Acoustic Sources (DAMAS) Determined from Phased Microphone Arrays,” 10th AIAA/CEAS Aeroacoustics Conference, Manchester, UK, AIAA-2004-2954, 2004.
[11] Blacondon, D., & Élias, G., “Level Estimation of Extended Acoustic Sources Using a Parametric Method,” *J. Aircraft*, vol. 41, no. 6, pp. 1360-136, Nov.-Dec. 2004.
[12] Casalino, D., Santini, S., Genito, M., & Ferrara V., “Rocket Noise Sources Localization through a Tailored Beam-Forming Technique,” *AIAA J.,* vol. 50, no. 10, pp. 2146-2158, Oct. 2012.
[13] Papamoschou, D. “Imaging of Directional Distributed Noise Sources,” *J. Sound & Vib*., vol. 330, pp. 2265-2280, 2011.
[14] Tam, C. K. W., Viswanathan, K., Ahuja, K. K. & Panda, J. “The sources of jet noise: experimental evidence,” *J. Fluid Mech.*, vol. 615, pp. 253-292, 2008.
[15] Zilliac, G., Waxman, B. S., Doran, E., Dyer, J., Karabeyoglu, M. A., & Cantwell, B., “Peregrine Hybrid Rocket Motor Ground Test Results,” *Joint Propulsion Conference*, AIAA paper 2012-4017, July 2012.